Fadallah *et al.*
Journal of Engineering and Applied Science (2022) 69:85
https://doi.org/10.1186/s44147-022-00141-0

Journal of Engineering and Applied Science

RESEARCH Open Access

Experimental investigation of small-scale shear walls under lateral loads

Reda Fadallah[1*], Mohamed Elbayomy[1], Hatem Ghith[2] and Hamed Salem[1]

*Correspondence:
reda.fadallah@eng.cu.edu.eg

[1] Faculty of Engineering, Cairo University, Giza, Egypt
[2] Housing & Building National Research Center, Giza, Egypt

Abstract

Shear walls are critical in designing of reinforced concrete structures against lateral loads. Although various research studies have been conducted on the design of reinforced concrete shear walls, these studies were limited by the laboratory capacity. This led to inability of testing walls with their full height for high to mid-rise shear walls. Fortunately, progress in specimen modeling techniques permitted performing scaled experimental studies. This paper presents 11 scaled down reinforced concrete shear walls—with 1/10 scale. The shear walls were cast to investigate various number of parameters. Shear walls have been tested under both monotonic and cyclic lateral loads. The scaled down tested specimens showed a behavior close to that of large-scale shear wall structural elements, not only in monotonic lateral loading, but also, in cyclic loading stiffness degradation and energy dissipation behavior. Experimental results were compared to that estimated by ACI sectional analysis as well as the ACI SP-36 and showed great similitude. The applicability to use the presented methodology is tested, in order to construct and test small-scale models of full-scale shear walls to allow for better understanding shear wall behavior under various loading conditions.

Keywords: Shear walls, Aspect ratio, Lateral loads, Drift, Small-scale testing, Cyclic loading

Introduction

A shear wall is a structural member designed to resist the lateral forces acting on a structure. These walls are critical in seismically active zones when shear forces on the structure increases due to earthquakes. Throughout the years, experimental investigation of shear wall behavior took place but mainly on squat shear walls. Experimental studies on low-aspect ratio walls ranging from 1 to 2 were done by Farrar and Baker and Salonikios et al. [1, 2]. Various parameters were studied on shear walls as applied in axial load, concrete type, steel grade, steel arrangement, and shear wall cross-section but mostly on squat shear walls [3–5]. Liao et al. and Salonikis et al. showed that the shear walls tested that have steel bars in the same direction as the principal direction of applied stresses in this study have greater ductility than that of conventional shear walls [2, 5]. While the prementioned studies focused on rectangular section shear walls, other studies investigated the effects of changing the cross-section of the wall. Ni et al.

studied two T-shaped shear walls, while Pinle et al. studied flanged shear walls with high strength stirrups [3, 4].

This type of walls which is usually controlled by shear failure behavior was experimentally tested because of their low rise, smaller size, lower cost, and convenience of testing equipment. Very few studies in literature investigated high to mid-rise shear walls, where flexure behavior is dominant, and as the aspect ratio increased for large-scale-sized specimen, the number of specimens decreased which was the case in numerous studies [6–8]. These studies were hindered by the higher cost of large-scale, high-rise shear walls, and the required testing setup and space. This clearly appeared in Aghniaey's study where the higher aspect ratio equals 3 was used to represent a 6-storey building. Using ¼ scale, only two large-scale specimens were implemented with aspect ratios of H/L = 2.0 and 3.0 [8].

To overcome these obstacles, a small-scale modeling was introduced. Different aspects of reinforced concrete modeling were studied over the years Janney et al. defined structural modelling as "a structural model is any structural element or assembly of structural elements built to a reduced scale (in comparison with full-size structures) which is to be tested and for which laws of similitude must be employed to interpret test results." [9]. This led researchers into investigating the different modeling techniques, to accurately represent the behavior of full-scale prototype, using small-scale model with minimal behavioral changes.

Mainly prototype concrete is a combination of cement, water, coarse, and fine aggregates, while model concrete consists of only fine aggregates, cement, and water [10]. By increasing the maximum aggregate size, the nominal compressive strength decreased; increasing the maximum aggregate size could increase the sensitivity of strength-to-structural size and make the size effect more obvious [11]. Brooks and Newman concluded that the mortar and concrete show the same elastic behavior on the stress-strain diagram, concrete nonlinear behavior starts at a lower stress than that of the mortar, both mortar and concrete shows a gradual curving with some ductility ahead of failure [12].

Many commercially available wires and rods exist and can be used as model reinforcement: round steel wire and rod, square steel rod, cold rolled threaded rods, deformed wires, commercially available, or custom deformed [10]. However, the main issue concerning model reinforcement is the bond characteristic. The bond between modal concrete and reinforcing rods were investigated, and the results showed that larger specimens with larger bars fail in a brittle, splitting mode, whereas smaller specimens with smaller bars fail in a less brittle, plastic shear-pullout mode [13].

As modeling techniques and obstacles were covered among the years, various researchers put size effect of reinforced concrete elements' behavior under test. The size effect of RC beams was studied experimentally. The findings of the investigation demonstrated that as the specimen size grows larger, the flexural compression strength, and final strain decreased [14]. Confirming the validity of small-scale models, Del Giudice et al. suggested constructing micro-RC specimens with a scale equal to 1/40, using a 3D printer. The tests were performed on cylinders, unreinforced and reinforced beams [15]. The tested properties seemed to resemble the ones of full-scale RC components. Other studies focused on size effects on shear wall specimens. Mortezaei and Kheyroddin

found that unlike shear walls with height to length ratio greater than 2, shear walls with less aspect ratio are shown to be free from size effect [16]. Moreover, Rasoolinejad and Bažant in a study on scaled down squat shear walls found that increasing the wall size may change the failure mechanism, cause the concrete to fail at a lower stress, and shorten or remove the yield plateau. Adding horizontal reinforcing bars to vertical ones tends to prevent inclined shear cracks in the web [17].

Research significance

Previous research showed that there is a need to further investigate high-aspect ratio shear wall behavior. Moreover, to overcome the limitation of the large specimen size, cost and testing equipment, advancement in scaling techniques allows for an alternative approach to understand high rise shear wall behavior at much lower specimen size and cost. The overall goal of this study is to investigate the behavior of scaled shear walls at a scale of 1:10 using available scaling techniques in literature to allow for increasing the tested aspect ratio of walls and a better understanding of modelled structural elements.

Experimental work and methodology

Test specimens

Eleven specimens were constructed to investigate various number of parameters including wall aspect ratio, vertical reinforcement ratio, horizontal reinforcement arrangement, and wall boundary. One specimen was tested under cyclic loading to report the cyclic behavior of scaled shear wall. To compare the modal specimens to a prototype of a larger scale shear wall, the work executed by Tasnimi on mid-rise walls was adopted. Four identical shear walls designed in compliance the ACI building code, with aspect ratio equals to three, were tested under quasistatic cyclic loading. The walls' dimensions are 1500×500×50 mm [18]. The geometrical scale between the prototype and the modal specimens is equal to 2.5. The prototype specimens were reinforced with a vertical flexural reinforcement ratio—at boundaries—1.8% equal to that of the cyclic specimen. All specimens were formed at 1/10 scale, with typical dimensions of width × length × thickness equals to 240×400×50 mm for the base and of height × length × thickness equals to 600×200×40 mm for the wall, except for the low-rise shear wall, with a wall dimension of 300×200×40 mm, high-rise shear wall, with a wall dimension of 900×200×40 mm, and the shear wall with concrete enlargement at its boundaries, with a concrete enlargement with dimension 80×40 at both shear wall ends. Main vertical reinforcement was 3 mm bars with 20 mm spacing, except for S1 with vertical reinforcement equals 2 mm in diameter, S7 with vertical reinforcement equals 4 mm in diameter, S8 with distributed vertical reinforcement equals 2 mm in diameter and concentrated 4 mm reinforcement at both ends, and S9 with distributed vertical reinforcement equals 2 mm in diameter and concentrated 4 mm reinforcement and concrete enlargement at both ends. The main horizontal reinforcements—stirrups—was 3mm closed stirrup bars with 20-mm spacing, except for S6 where the bond effect off the stirrups was studied by using U-shaped stirrups, S2 with inclined stirrups at 45° with no boundary vertical reinforcement, and S10 with inclined stirrups at 45° with boundary vertical reinforcement. Table 1 illustrates the characteristics of the tested specimens. Examples for specimens detailing are shown in Fig. 1. Notably, extended development length of the vertical bar

Table 1 Specimens' characteristics

Specimen name	Aspect ratio	Vertical reinforcement diameter	Horizontal reinforcement arrangement	Boundary elements	Cyclic loading
S1	3	2 mm	Closed/straight	No	No
S2	3	3 mm	Inclined	No	No
S3	1.5	3 mm	Closed/straight	No	No
S4	3	3 mm	Closed/straight	No	No
S5	4.5	3 mm	Closed/straight	No	No
S6	3	3 mm	U-shaped stirrups	No	No
S7	3	4 mm	Closed/straight	No	No
S8	3	4 mm concentrated and 2 mm distributed	Closed/straight	Yes	No
S9	3	4 mm concentrated and 2 mm distributed	Closed/straight	Yes	No
S10	3	4 mm concentrated and 2 mm distributed	Inclined	Yes	No
S11	3	3 mm	Closed/straight	No	Yes

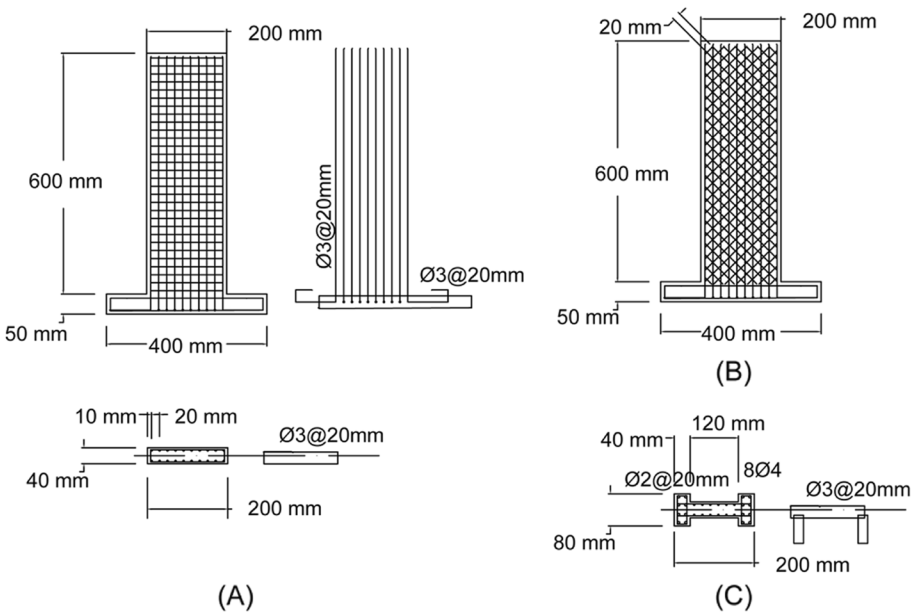

Fig. 1 **A** Typical reinforcement detailing for scaled shear wall, **B** reinforcement detailing for inclined stirrups, and **C** cross-section of shear wall with end enlargement and steel concentration

was implemented to prevent any slippage due to the use of smooth bars as shown in Fig. 1.

Methods

Generally, rules of similitude that should be satisfied are geometric similitude and similar stress strain curves for modal material to that of the prototype, which is necessary for ultimate loading condition as for this study. Moreover, one can ensure full similitude between reinforced concrete model and prototype by obeying the following similitude equation derived from dimensional analysis by Noor and Boswell [19].

$$S_Q = \frac{Q_p}{Q_m} = \frac{\sigma_p}{\sigma_m}\left(\frac{l_p}{l_m}\right)^2 = S_\sigma \cdot S_l^2 \quad (1)$$

where S_Q = The concentrated load scale
Q_p = The prototype load
Qm = The model load
σ_p = The prototype material strength
σ_m = The model material strength
l_p = The prototype geometrical length
l_m = The model geometrical length
S_σ = The strength scale between the prototype and the model
S_l = The geometrical scale between the prototype and the model

However, since the model specimen consists of two distinctive materials and steel is the only feasible material for practical modeling, thus the strength scale could be taken equal to steel strength scale [19].

Clean and rounded siliceous sand was used in the mixture. Appropriate sieve analysis was conducted to ensure the accurate representation of coarse and fine sand particles to resemble that of the prototype. No accepted rules are available to determine the maximum aggregate size for model concrete, but it may be also obtained from the model geometric scale, the minimum member thickness, and the reinforcements spacing [10]. The nominal aggregate size is 2.36 mm compared to a size of 10 mm for that of the prototype, allowing for proper casting of the walls despite the narrow spacing between bars, while also ensuring reaching the required compressive strength. Finesse modulus was calculated to be 3.08 (2.9–3.2) (i.e., coarse sand). In addition, cumulative percentage passing from sieve 0.6 mm was 34% (<35%). Thus, it was considered coarse sand.

The average cylinder strength for the prototype strength is equal to 22.3 Mpa, which was equivalent to cube strength of 28 Mpa. Thus, trial mixes were tested and the chosen mix was designed to develop cube compressive strength of 30 MPa after 28 days. The tested mortar cube side was 70 mm. The ratio of the mortar by weight was cement to water to sand = 0.42:1:1.68, and the required weights to cast 1 m^3 of concrete with the required strength are 350 kg cement, 170 kg water, and 1260 kg sand.

Commercially available high-grade steel rebars were used as the main reinforcing bars for the wall and its base. Notably, the bars with smaller diameter had higher strength than that of larger ones; 2 mm, 3mm, and 4mm bars showed yield stress of 900 Mpa, 600 MPa, and 500 MPa, respectively, and ultimate strength of 937 Mpa, 678 Mpa and 623 Mpa, respectively. The yield strength of the prototype was equal to 276 Mpa, and the steel strength scale was included in the comparison between the cyclic modal specimen and the prototype as mentioned in Eq. (1).

Mixing and casting

According to the specimens' dimensions, the wooden forms were constructed and the reinforcement cages were assembled as designed as shown in Fig. 2A and B. The concrete mixture components are weighted and added to the mixer, with the following order: first dry components including coarse aggregate, then fine aggregate, then cement, then mixed for 1~2 min, and afterwards, the water is added. Mixing lasted till

Fig. 2 **A** Reinforcement detailing for S9 and **B** reinforcement detailing for S2

the mixture became homogenous. The forms were then coated with oil before casting, the reinforcement mesh is placed inside the wooden form, and pipes are inserted at the predetermined bolt's locations. The mixture is then casted in the wooden forms and the shaking table is used for compaction, and the specimens' surface was leveled. The forms were removed after 24 h from casting. Specimens were then cured by immersion in water for 4 weeks.

Test setup

The test was executed in the small-scale modeling laboratory in the reinforced concrete laboratory of the Faculty of Engineering, Cairo University. Specimens were anchored to the testing table using eight 14-mm bolts. The load was applied by a jack in a horizontal direction with a capacity of 25 kN. The load was applied with a rate of 1 kN per minute. No axial load was applied to the specimen because for the aspect ratio used for the tested walls axial stresses is a small relative to the walls' capacity. The deflection was measured by a horizontal LVDT, with maximum deformation capacity of 50 mm. The test setup is shown in Fig. 3. The loading procedure stopped, and the unloading procedure commenced after the load cell value dropped to about 95% of that of the ultimate load.

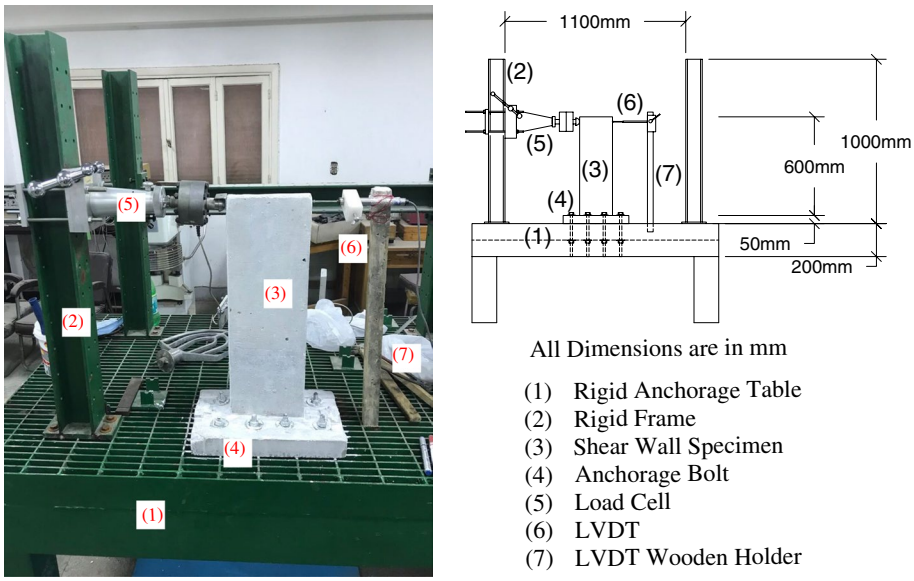

Fig. 3 Test setup

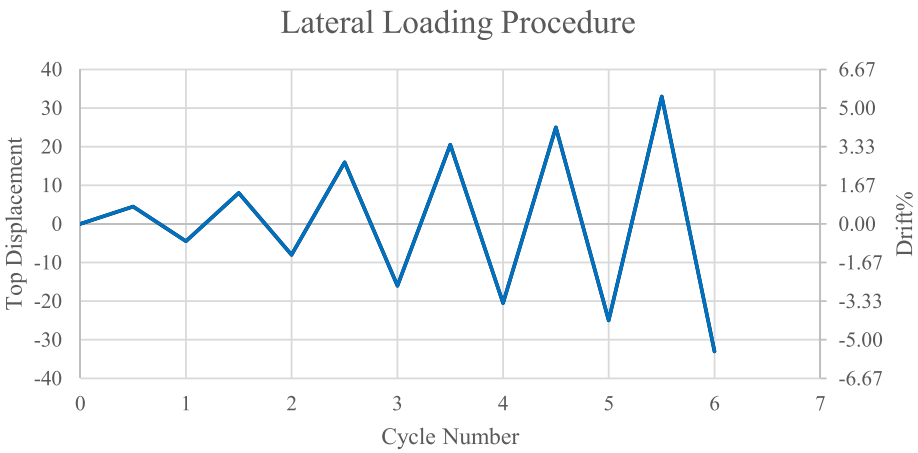

Fig. 4 Cyclic loading procedure of S11

In Fig. 4, the cyclic loading procedure for S11 is illustrated, where 6 cycles of loading took place as shown. The cycles were considered multiples of the yield drift which is equal to 2.2%.

Results and analysis

Table 2 summarizes the test results of the first ten specimens tested under monotonic loading. The results include the mode of failure, initial cracking load (Pi) and its corresponding deformation (Δi), yield load (Py) and its corresponding deformation (Δy), and finally ultimate load (Pu) and its corresponding deformation (Δu). Loads are in N, while deformations are in millimeter. Initial cracking on specimens was identified by both visual inspection and change in the stiffness of the load-deflection curves. Notably,

Table 2 Summary of the shear wall specimens test results

Specimen	Mode of failure	Pi	Δi	Py	Δy	Pu	Δu
S1	Flexural shear failure	2747	2.30	7523.68	12.88	8660.27	27.58
S2	Flexural failure	4218	6.45	8828.61	14.57	9467.24	15.90
S3	Shear failure	8142	8.08	17165.93	68.85	19054.06	86.61
S4	Flexural shear failure	2158	2.35	7714.29	13.04	8861.47	58.79
S5	Flexural failure	294	0.42	5943.68	23.17	6642.55	34.61
S6	Flexural shear failure	3335	3.59	7443.53	12.27	8483.69	16.73
S7	Flexural failure	4316	2.94	10539.86	9.49	11266.88	14.07
S8	Flexural shear failure	1570	1.65	9944.10	16.37	10864.28	24.69
S9	Flexural failure	4218	2.34	11584.43	12.00	13464.32	15.79
S10	Flexural failure	1962	1.52	8571.68	11.44	9724.55	16.10

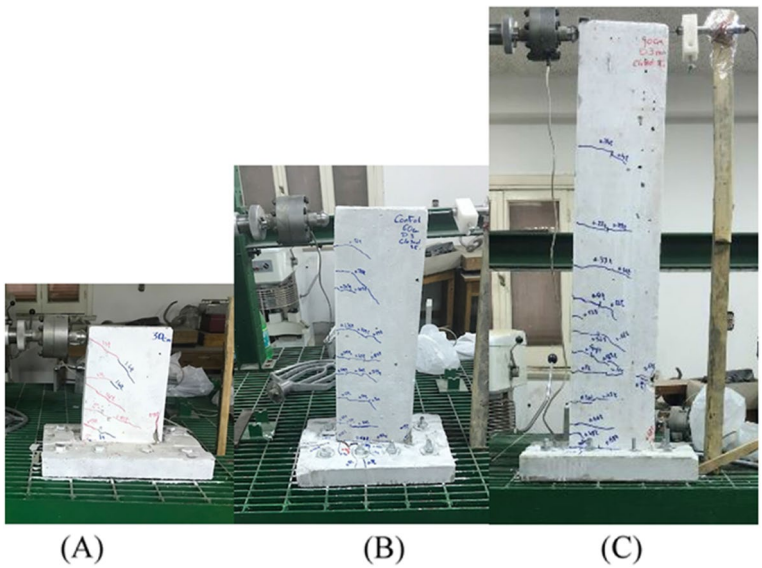

Fig. 5 Shear walls with varying aspect ratio from **A** R= 1.5, **B** 3, and **C** 4.5

the yield deformation was obtained using the secant method. First, a secant was defined by the origin and where a horizontal line defined by 75% of the maximum applied load intersected the curve. The yield displacement was then defined by where the secant intersected the horizontal defined by the maximum applied load.

Effect of shear wall aspect ratio

This group contains 3 specimens S3, S4, and S5. The aspect ratios are 1.5, 3, and 4, respectively. The failure modes for specimens S3, S4, and S5 were considered shear failure, flexural shear failure, and flexural failure, respectively. S3 has higher initial crack load value by 277.3% than that of S4 and S4 has higher initial crack load value by 633.3% than that of S5. This is due to the higher stiffness for low-rise walls compared to higher walls. In Fig. 5, crack pattern for the three specimens is compared. These results agreed with the experimental and analytical results obtained by Aghniaey stated that by

increasing the wall's aspect ratio, the dominant failure mode changes from shear failure to flexure failure [8].

The load deflection curves generally show three main stages with significant changes in the slope of the curve. The first stage starts from initial loading up to cracking load and has nearly linear behavior, referred to as uncracked behavior. The second stage starts from cracking load and is characterized by reduction in stiffness until reaching maximum horizontal load. The third stage is considered the plastic behavior that the wall undergoes and characterized with large deformations. Figure 6 illustrates the load-deflection curves for specimens under consideration. S3 could not be unloaded due to excessive deformations acquired by the specimen, exceeding the LVDT's limit.

For demonstrating the effect of changing wall's aspect ratio, ultimate load values between specimen are compared. Ultimate load values for the specimens under consideration are higher in S3 than that of S4 by 115.02% and are higher in S4 than that of S5 by 33.4%. This can be attributed to the larger stiffness of low-rise walls in comparison to higher walls.

Effect of shear wall vertical reinforcement ratio

This group contains 3 specimens S1, S4, and S7. Their main vertical reinforcing bars were 2 mm in diameter, 3 mm, and 4 mm, respectively.

The failure mode for specimens S1, S4, and S7 was considered flexural shear failure, flexural shear failure, and flexural failure, respectively. The increasing of the walls' vertical reinforcement ratio changes the dominating mode of failure from flexural shear to flexural failure. S1 has slightly higher initial crack load value by 27.3% than that of S4 and S7 has higher initial cracking load value by 100% than that of S5. In Fig. 7, crack pattern for the three specimens is compared.

The load deflection curves generally show the same behavior as previously mentioned in previous group of specimens. Figure 8 illustrates the load-deflection curves for specimens under consideration. The main reason for discrepancies between the specimens'

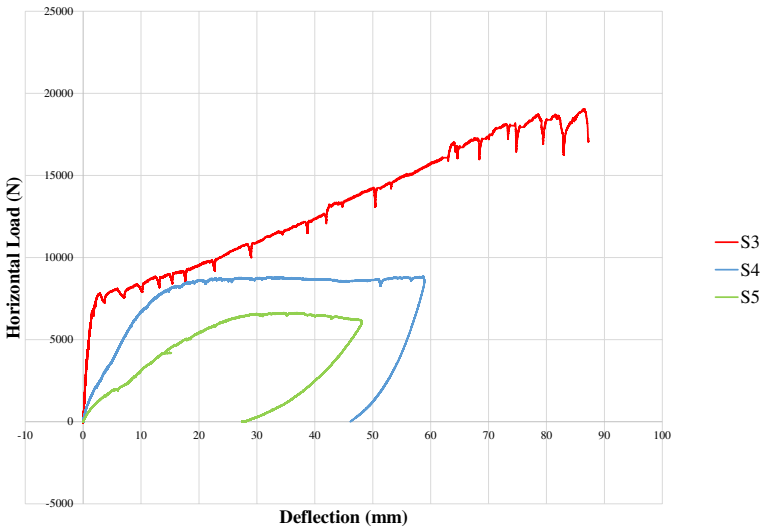

Fig. 6 Load deflection curve for specimens: S3, S4, and S5

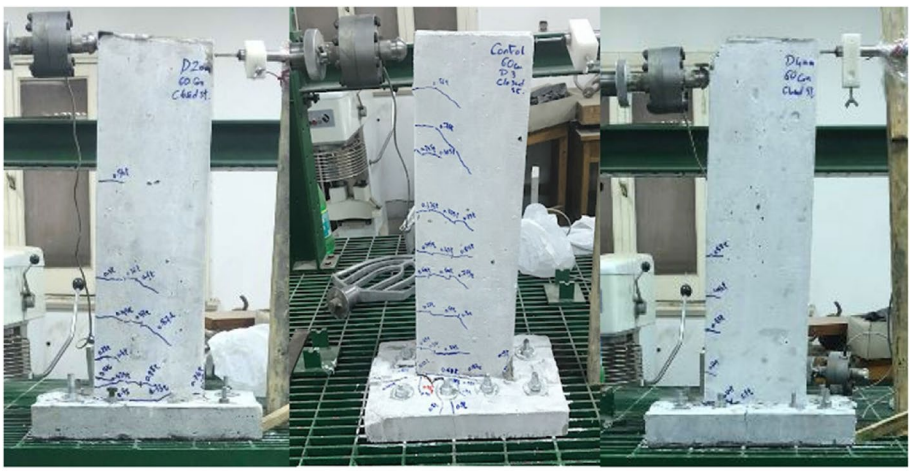

Fig. 7 Walls with varying vertical RFT from **A** D= 2mm, **B** 3mm, and **C** 4mm

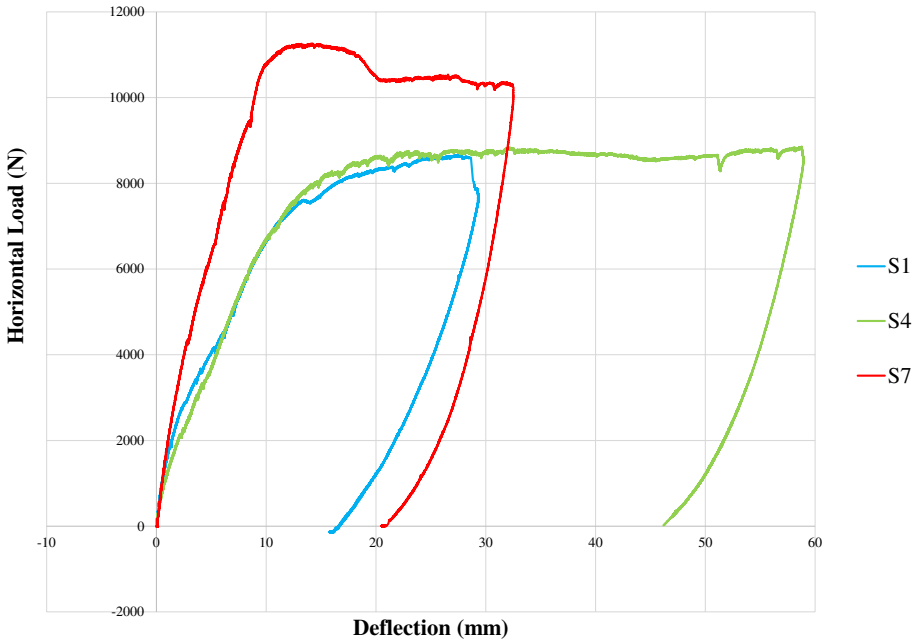

Fig. 8 Load deflection curve for specimens: S1, S4, and S7

load deflection behavior is the higher strength for smaller diameter bars as mentioned in the "Methods" section, where a smaller diameter has higher yield and ultimate tensile strengths.

Ultimate load values for the specimens under consideration is higher in S7 than that in S4 and S1 by 27.14% and 30.1%, respectively. On the other hand, ultimate load values were nearly equal in S1 and S4, and this may be attributed to higher yield strength values for smaller bar diameters versus lower yield value for larger bar diameter.

Effect of shear wall horizontal reinforcement arrangement

This group contains 4 specimens S2, S4, S6, and S10. S2 had inclined 3-mm stirrups with 3-mm bars vertical reinforcement, S4 had closed horizontal 3-mm stirrups with 3-mm bars vertical reinforcement, S6 had horizontal U-shaped stirrups with 3-mm bars vertical reinforcement and finally, and S10 had inclined 3-mm stirrups with concentrated 4-mm vertical reinforcement bars and distributed 2-mm vertical reinforcement bars. The main parameter changing in this group is the effect of changing the horizontal reinforcement arrangement. Other researchers such as Zhang et al. and Liao et al. introduced the idea of adding inclined reinforcement for a better behavior of shear wall in resisting lateral loads. This construction measure enhanced the lateral load resisting behavior as the bars are added in the direction of applied principal stresses [5, 20]. In this study, small-scaled specimens allowed for easily deforming and arrangement steel bars, thus experimenting the addition of inclined stirrups to the vertical bars as well.

The failure mode for specimens S2, S4, S6, and S10 was considered flexural failure, flexural shear failure, flexural shear failure, and flexural failure, respectively. Adding inclined stirrups instead of horizontal stirrups clearly changes the dominating mode of failure from shear to flexural failure and prevent appearing of diagonal shear cracks. S2 has higher initial crack load value by 95.45% than that of S4. S6 has higher initial crack load value by 54.55% than that of S4. S4 has slightly higher initial crack load value by 10% than that of S10. In Fig. 9, the crack pattern for the three specimens is compared.

The load deflection curves generally show the same behavior as previously mentioned in the previous group of specimens. Figure 10 illustrates the load-deflection curves for specimens under consideration. Although ductility of S10, with inclined stirrups and concentrated reinforcement, is higher than that of S2 and S6 as expected, S4 had the highest ductility amongst them. This was attributed to higher stiffness of S2 and S10 using inclined stirrups opposing horizontal stirrups in S4 resulting in relatively less deformations and thus less ductility. Moreover, S4 using closed stirrups allowed for higher deformations to take place opposing U-shaped stirrups in S6.

Ultimate load values for the specimens under consideration were nearly equal in the four specimens. Ultimate load value is higher in S10 than that of S2, S4, and S6 by 2%,

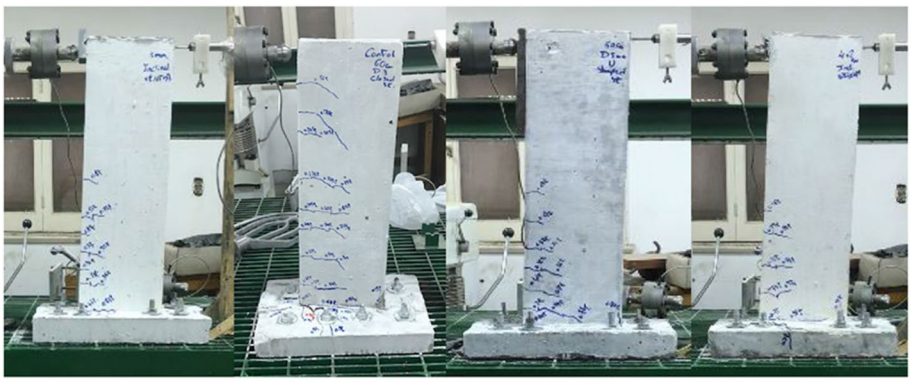

Fig. 9 Walls with varying stirrup detailing from **A** inclined stirrups with 3mm VL RFT, **B** closed stirrups, **C** U-shaped stirrups, and **D** inclined stirrups with 4+2mm VL RFT

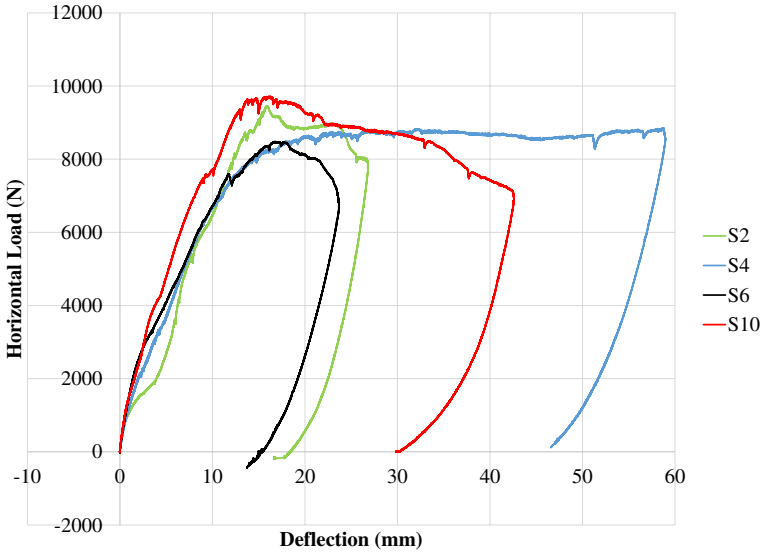

Fig. 10 Load deflection curve for specimens: S2, S4, S6, and S10

9.74%, and 14.63% respectively. The horizontal reinforcement arrangement had a minor effect on wall capacity but had a major effect on the walls' mode of failure as prementioned in cracking pattern comparison.

Effect of shear wall boundary elements

This group contains 3 specimens S4, S8, and S9. S4 had no boundary elements with only 3-mm vertical reinforcement. S8 had concentrated 4-mm vertical reinforcement and distributed 2-mm vertical reinforcement. S9 had both concentrated 4-mm vertical reinforcement and distributed 2-mm vertical reinforcement and concrete enlargements 4×8 cm at wall ends as well. The main parameter changing in this group is the effect of adding boundary elements on shear wall.

The failure mode for specimens S4, S8, and S9 was considered flexural shear failure, flexural shear failure, and flexural failure, respectively. Adding boundary elements to the wall ensured ductile flexural failure, but did not prevent diagonal shear cracks. S4 has higher initial crack load value by 37.5% than that of S8 and S9 has higher initial crack load value by 95.45% than that of S4. In Fig. 11, the crack pattern for the three specimens is compared.

The load deflection curves generally show the same behavior as previously mentioned in previous group of specimens. Figure 12 illustrates the load deflection curves for specimens under consideration. Although S8 and S9 had boundary elements, S4 had the highest ductility amongst them. This was attributed to higher stiffness of S8 and S9 leading to relatively less deformations and thus less ductility.

Ultimate load values for the specimens under consideration clearly increased by adding boundary elements in the wall. S9 had higher ultimate load than that of S8 and S4 by 23.93% and 51.94%, respectively.

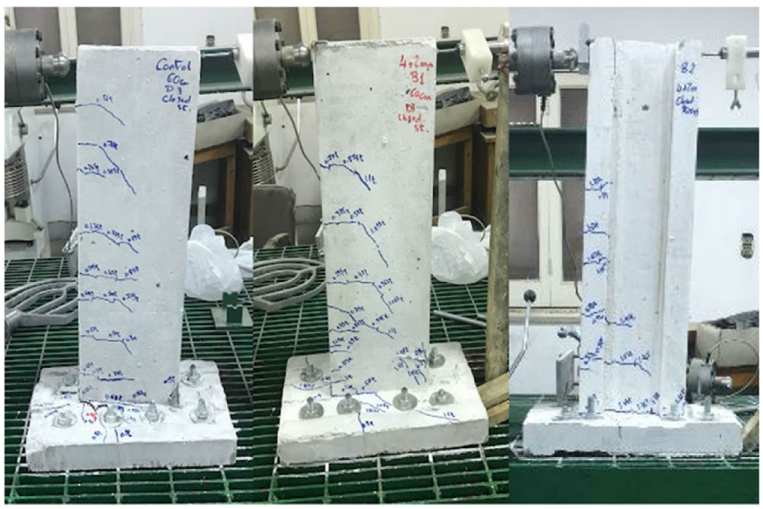

Fig. 11 Shear walls with varying boundary element detailing from **A** non-concentrated 3-mm RFT, **B** concentrated 4mm and distributed 2mm, and **C** concentrated 4mm and concrete enlargement and distributed 2mm

Shear wall cyclic behavior

In S11, the horizontal loading was changed from monotonic to cyclic. S11 both had 3-mm vertical reinforcement and 3-mm horizontal reinforcement. Figure 13 illustrates the hysteresis loop curves. The specimen initially was free of cracks in the first cycle until reaching a horizontal load value of 3628 N. In the opposite direction, the initial cracking load was less with a value of 1726 N. For the first loading

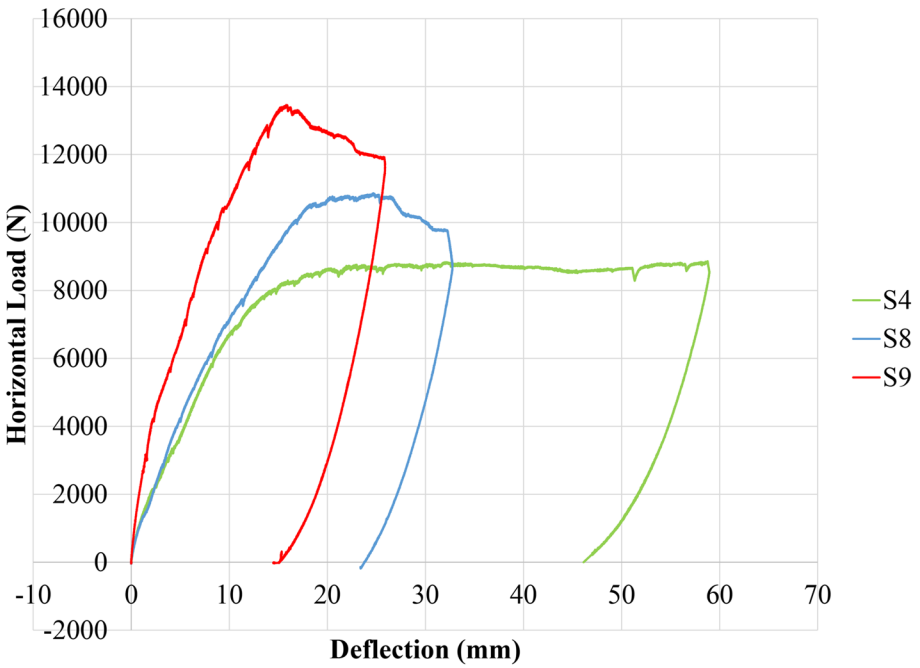

Fig. 12 Load deflection curve for specimens: S4, S8, and S9

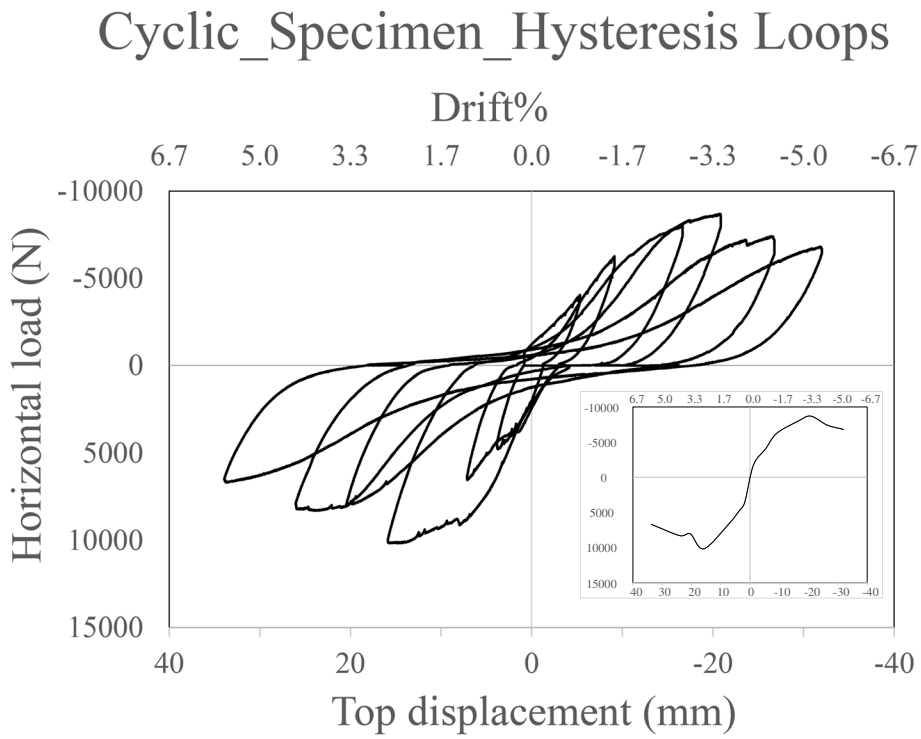

Fig. 13 Hysteresis loops of the cyclic specimen

cycle, maximum load was 4786 N and 4050 N in the opposite direction. For the second loading cycle, the maximum load was 6561 N and 6257 N in the opposite direction. For the third loading cycle, the maximum load was 10,179 N and 8022 N in the opposite direction, and the specimen reached yielding point, followed by concrete crushing at the end of the cycle. For the fourth loading cycle, maximum load reached was 8041 N and 8698 N in the opposite direction, with no additional cracks, only widening of existing cracks. For the fifth loading cycle, maximum load reached was 8316 N and 7414 N in the opposite direction, as well as a breaking sound was heard due to crushing of concrete in compression and no additional cracks appeared, only widening of existing cracks occurred. For the sixth loading cycle, the maximum load reached was 6708 N and 6806 N in the opposite direction, with no additional cracks, only widening of existing cracks. The crack pattern for each cycle appears in Fig. 14. The prementioned results and behavior agreed with the description of cyclic loading behavior for large-scale specimen executed by Ni et al. as well as most of the cyclic loading experiments in literature [6].

Discussion

Model versus prototype

The concentrated load values were compared between S11 and the four specimens tested by Tasnimi SHW1, SHW2, SHW3, and SHW4 at the same drift value. The results shown in Table 3 showed that the model specimen obeyed the similitude Eq. (1) to a great extent.

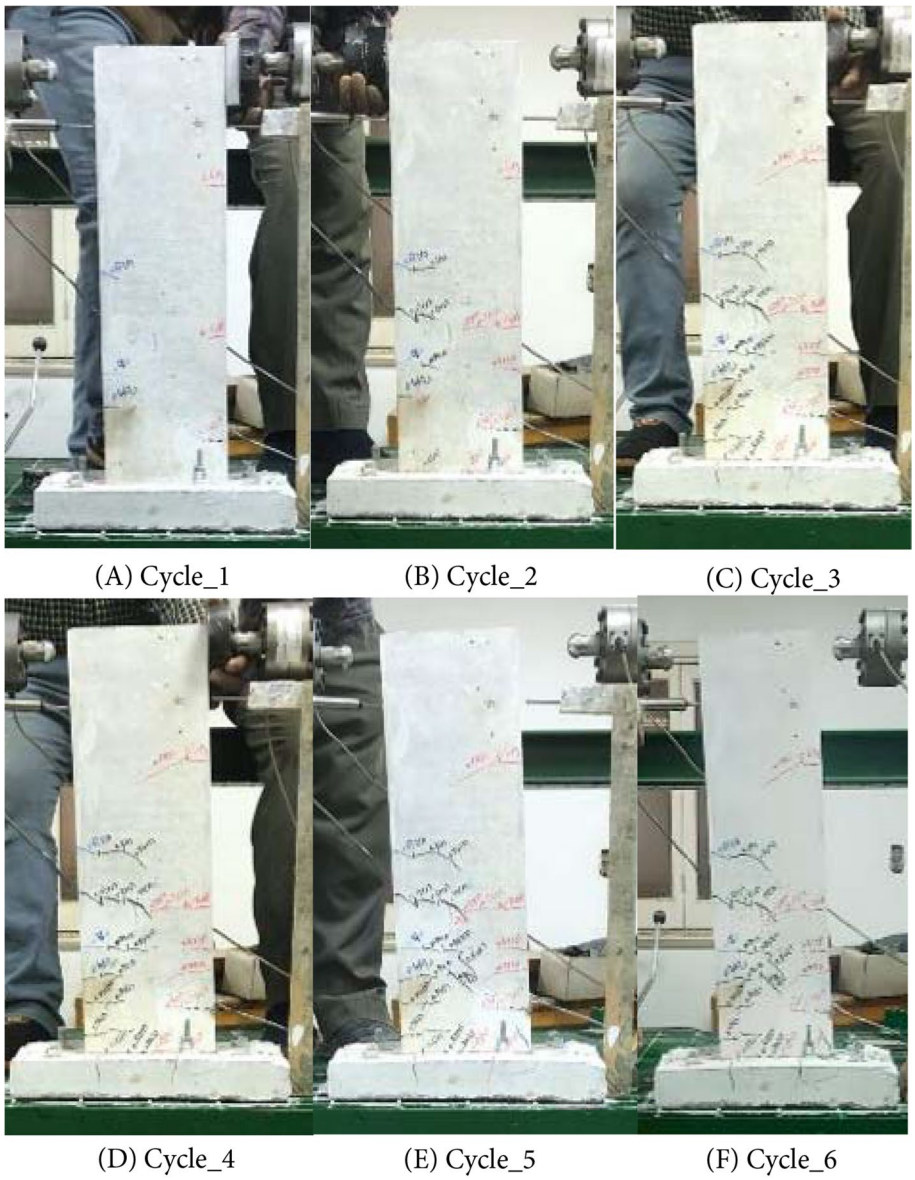

Fig. 14 The crack pattern after each loading cycle **A** first cycle, **B** second cycle, **C** third cycle, **D** fourth cycle, **E** fifth cycle, and **F** sixth cycle

Table 3 Comparison between modal specimen S11 and SHW1 SHW2, SHW3, and SHW4 at a drift percentage of 1%

Specimens	Prototype load (N)	Model load (N)	Percentage of variation
S11	---	6042.96	---
SHW1	15420	5365.23	11%
SHW2	19560	6805.7	13%
SHW3	17500	6088.94	1%
SHW4	19760	6875.3	14%

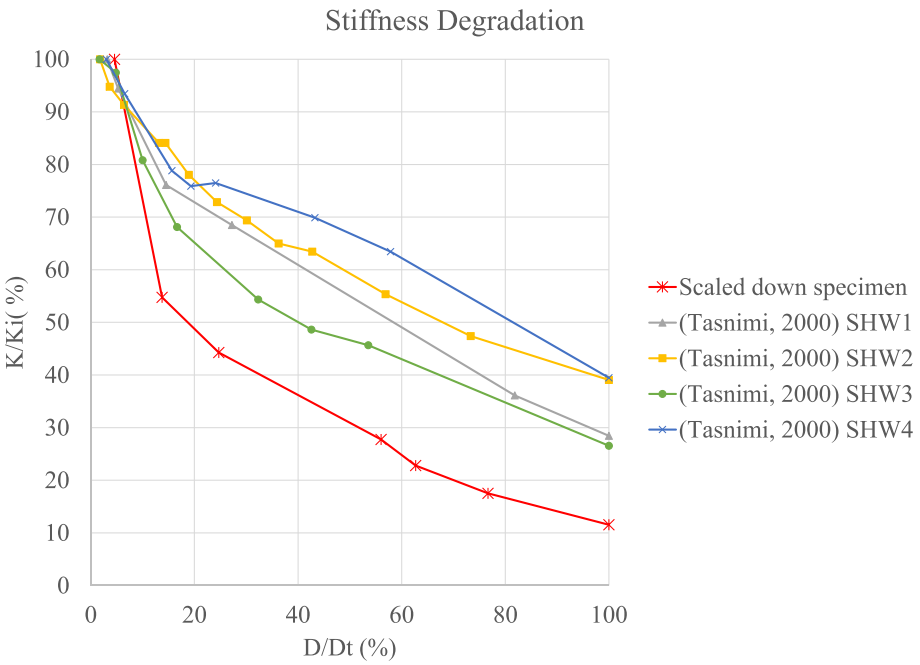

Fig. 15 Stiffness degradation comparison

Stiffness degradation

Figure 15 shows the stiffness degradation curve for the specimens S11, with the four specimens tested by Tasnimi [18]. The horizontal axis is the relative drift percentage and the vertical axis is the relative secant stiffness to the initial stiffness of the wall, as follows:

$$\boldsymbol{Ki} = \frac{|-\boldsymbol{Pi}| + |+\boldsymbol{Pi}|}{|-\boldsymbol{Xi}| + |+\boldsymbol{Xi}|} \tag{2}$$

where +Pi and −Pi are the positive and negative lateral peak loads, respectively, of the *i*th hysteretic loop and +Xi and −Xi are the positive and negative lateral top displacement, respectively, of the *i*th hysteretic loop. This illustrates the decrease in the stiffness after each loading cycle with additional crack initiation and widening. The shown graph shows same pattern in declining stiffness of the wall specimens under consideration after normalization, in both scaled down specimen and large-scale specimen.

Energy dissipation capacity

Energy dissipation was calculated similarly to Li et al., where in the mentioned study, the cumulative energy consumption Ep is defined as the area enclosed by all loading cycles' hysteresis curves until the drift ratio reaches a specified threshold during the first loading cycle, which can reflect the real dissipated energy of specimens during the loading process [7]. Figure 16 illustrates the cumulative energy dissipation pattern for both curves till reaching 100% of their respective drifts. The curves indicate similar energy consumption rate in both small- and large-scale shear wall specimens. Minor differences occurred at the end of the loading cycles between large-scale and

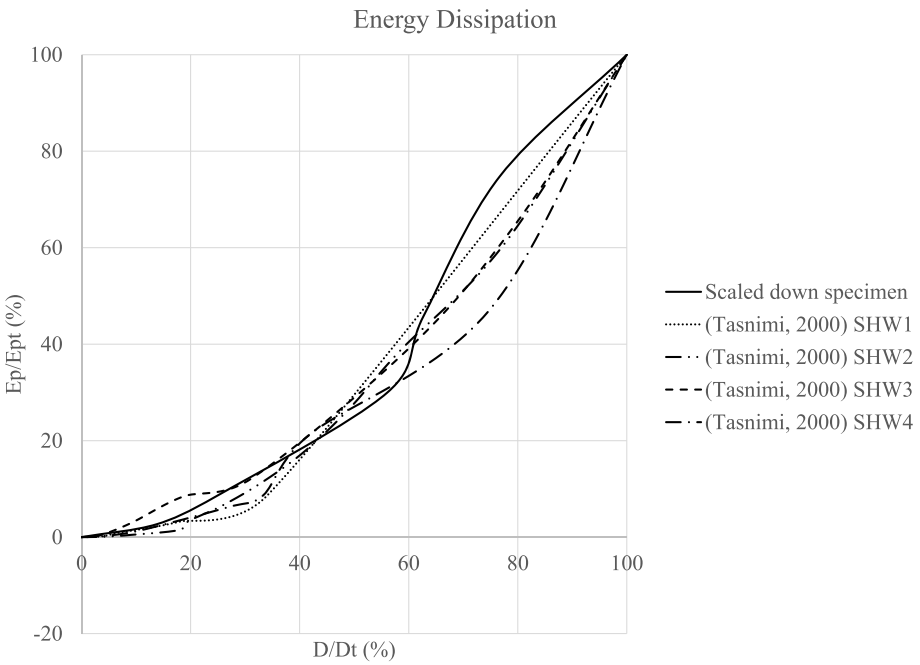

Fig. 16 Cumulative energy dissipation comparison

small-scale wall behavior, which may be attributed to fewer number of cracks relative to large scale models, which may lead to different energy consumption rate along final loading cycles.

Experimental results versus ACI sectional analysis and ACI approximate estimations

The experimental failure loads were compared to ACI 318 sectional analysis as well as that estimated by the following equation, proposed by ACI SP-36 [21], which can be used to compute the approximate moment capacity of rectangular shear walls with uniformly distributed vertical reinforcement. Thus, S8, S9, and S10 were omitted from

Table 4 Comparison between theoretical results and experimental results for scaled down shear walls

Specimens	Experimental results (N)	ACI sectional analysis (N)	Percentage of variation	ACI SP-36 (N)	Percentage of variation
S1	8660.3	8298.0	-4%	9230.9	7%
S2	9467.2	9589.4	1%	10248.4	8%
S3	19054	19178.9	1%	20496.8	8%
S4	8861.5	9589.4	8%	10248.4	16%
S5	6642.5	6393.0	-4%	6832.3	3%
S6	8483.7	9589.4	13%	10248.4	21%
S7	11267	12188.0	8%	13037.5	16%
S8	10864	9349.2	-14%	---	---
S9	13464	16050.4	19%	---	---
S10	9724.6	9321.4	-4%	---	---

comparison as they had boundary elements. The load capacity was calculated by dividing the Mu by the shear wall's arm for each specimen.

$$M_u = \Phi \left[0.5 A_s f_y l_w \left(1 + \frac{P_u}{A_s f_y} \right) \left(1 - \frac{C}{l_w} \right) \right] \tag{3}$$

Where $\frac{C}{l_w} = \frac{\omega+\alpha}{2\omega+0.85\beta_1}$ $\omega = \frac{A_s f_y}{l_w h f_c'}$ and $\alpha = \frac{P_u}{l_w h f_c'}$

C= distance from the extreme compression fiber to the neutral axis

As = total area of vertical reinforcement

lw = horizontal length of wall

Pu = factored axial compressive load

fy = yield strength of reinforcement

Φ = strength reduction factor taken equal to 1

h = thickness of shea wall

β_1 = 0.85 for strength fc up to 281.0 kg/cm^2 and reduced continuously to a rate of 0.05 for each 70 kg/cm^2 of strength in excess of 281.0 kg/cm^2

Table 4 shows the difference between experimental and analytical results. The variations range between nearly 3% and 21% for the approximate equation; the maximum difference occurred in S6. The use of U-shaped stirrups in S6 caused the capacity of the wall to decrease—opposing closed and inclined closed stirrups—and Eq. (2) gave an overestimate for the wall's flexural capacity. Further numerical analysis is required to add the mentioned parameters to the shear wall design process. However, comparing the experimental results to traditional ACI sectional analysis resulted in variations ranging from −14 up to 19%. Maximum variations are −14% and 19% occurred in S8 and S9, respectively, which may be attributed to non-consideration of confining stirrups surrounding boundary concentrated reinforcement at wall ends.

Conclusions

This research proposed scaling the shear walls to 1/10 scale to allow for testing larger number of specimens with larger aspect ratio. The scaled down tested specimens showed a behavior close to that of large-scale shear wall prototype, not only in monotonic lateral loading, but also, in cyclic loading stiffness degradation and energy dissipation behavior. Therefore, it is applicable to use the presented methodology to construct and test small-scale models of full-scale shear walls to allow for better understanding of the shear wall behavior under various loading conditions. Monotonic testing for scaled down walls agreed to a great extent, with ACI sectional analysis as well as the ACI SP-36 flexural capacity equation for rectangular shear walls with uniformly distributed vertical reinforcement [21]. Increasing the aspect ratio from 1.5 to 3 and 4.5 changed the mode of failure of the wall from shear failure to combined flexural shear failure and flexural failure. Increasing vertical reinforcement ratio increased load capacity as expected. Changing horizontal bar arrangement to inclined stirrups had minor effect on wall capacity, but major effect on wall's mode of failure as inclined bars prevented appearance of inclined shear cracks in the specimens.

Acknowledgements
Not applicable.

Authors' contributions
Methodology, investigation, and writing: RF. Supervision, guidance, and review: MB, HG, and HS. The authors have read and approved the manuscript.

Funding
No funding was obtained for this study.

Availability of data and materials
The data presented are available on request from the corresponding author.

Declarations

Competing interests
The authors declare that they have no competing interests.

Received: 12 June 2022 Accepted: 8 September 2022
Published online: 24 September 2022

References

1. Farrar CR, Baker WE (1993) Experimental assessment of low-aspect-ratio, reinforced concrete shear wall stiffness. Earthquake Eng Struct Dyn 22:373–387
2. Salonikios TN, Kappos AJ, Tegos IA, Penelis GG (2000) Cyclic load behavior of low-slenderness reinforced concrete walls: failure modes, strength and deformation analysis, and design implications. ACI Struct J 97:132–141
3. Pinle Z, Junxiong L, Gan Z (2021) Seismic behavior of flanged reinforced concrete shear walls with high-strength stirrup under cyclic loading. Struct Design Tall Spec Build 30:e1844
4. Ni X (2021) Hysteretic behavior of T-shaped walls reinforced by high-strength bars: cyclic loading tests and modelling. In: Structures
5. Liao W-I, Zhong J, Lin CC, Mo YL, Loh C-H (2004) Experimental studies of high seismic performance shear walls. In: Proc. of 13th World Conf. on Earthquake Engineering
6. Ni X, Cao S, Liang S, Li Y, Liu Y (2019) High-strength bar reinforced concrete walls: cyclic loading test and strength prediction. Eng Struct 198:109508
7. Li X, Zhang J, Cao W (2020) Hysteretic behavior of high-strength concrete shear walls with high-strength steel bars: experimental study and modelling. Eng Struct 214:110600
8. Aghniaey N (2021) Behaviour of concrete shear walls reinforced with high-strength reinforcement under reversed cyclic loading
9. Janney JR, Breen JE, Geymayer H, Lockman WT, Rocha M (1970) The use of models in structural engineering. Spec Publ 24:1–18
10. Harris HG, Sabnis G (1999) Structural modeling and experimental techniques. CRC press
11. Jin L, Yu W, Li D, Du X (2021) Numerical and theoretical investigation on the size effect of concrete compressive strength considering the maximum aggregate size. Int J Mech Sci 192:106130
12. Brooks AE, Newman K (1968) The structure of concrete and its behaviour under load: proceedings of an international conference, London, September 1965. Cement & Concrete Association of Great Britain
13. Bazant ZP, Sener S (1988) Size effect in pullout tests. ACI Mater J 85:347–351
14. Yi S-T, Kim M-S, Kim J-K, Kim J-HJ (2007) Effect of specimen size on flexural compressive strength of reinforced concrete members. Cement Concrete Composites 29:230–240
15. Del Giudice L, Wrobel R, Leinenbach C, Vassiliou M (2020) Testing of additively manufactured small scale rc specimens for statistical validation of structural models in earthquake engineering. In: 11th International Conference on Structural Dynamics, EURODYN 2020 (virtual)
16. Mortezaei A, Kheyroddin A (2009) Size effects in reinforced concrete flanged shearwalls. Int J Civil Eng 7:27–40
17. Rasoolinejad M, Bažant ZP (2019) Size effect of squat shear walls extrapolated by microplane model M7. ACI Struct J 116:75–84
18. Tasnimi AA (2000) Strength and deformation of mid-rise shear walls under load reversal. Eng Struct 22(4):311–322
19. Noor FA, Boswell LF (1992) Small scale modelling of concrete structures. CRC Press
20. Zhang J, Liu J, Li X, Cao W (2021) Seismic behavior of steel fiber-reinforced high-strength concrete mid-rise shear walls with high-strength steel rebar. J Bldg Eng 42:102462
21. Cardenas A, Magura DD (1973) Strength of high-rise shear walls-rectangular cross section. In: Response of Multistory Concrete Structures to Lateral Forces, ACI Publication SP-36. American Concrete Institute, Detroit

Publisher's Note